Journal of Sound and Vibration (2000) **237**(1), 1–21
doi:10.1006/jsvi.2000.3059, available online at http://www.idealibrary.com on IDEAL®

THE EFFECT OF STRUCTURAL ELASTICITY ON THE EFFICIENCY OF NOISE BARRIERS

P. JEAN

Centre Scientifique et Technique du Bâtiment, 24 *rue Joseph Fourier*, 38400 *Saint-Martin-d'Hères*, *France*, *E-mail*: *jean@cstb.fr*

(*Received* 5 *July* 1999, *and in final form* 21 *January* 2000)

The efficiency of noise barriers is usually estimated neglecting their elastic behaviour. In this paper, the total vibro-acoustical response of simple barriers is considered. A variational approach with a boundary-element technique is used. It is a generalization of an existing formalism developed for the study of two-dimensional acoustical problems. The case of straight and thin barriers is studied. It is found that, at low frequencies, their vibrations can modify their insertion losses by several decibels.

1. INTRODUCTION

Important efforts are being made in order to improve both the efficiency and the design of noise barriers. Straight and thick barriers are replaced by more sophisticated ones with improved shapes. Thin wood or glass panels are now employed. New caps to place at their top are being tested [1]. Many parameters have been considered so far when assessing the efficiency of noise barriers: geometry [2], type of ground [3], type of source [4–7], complex interactions with surroundings such as the body of a train [6, 8], and atmospheric conditions [9, 10]. Vibration of the noise barrier is usually considered to be of no importance. This implies that the transmission is due solely to diffraction effects at the top of the barrier, and that transmission through the barrier can be neglected. This assumption seems quite reasonable in the case of thick concrete or brick walls, for instance; however, the effect of transmission seems worth considering when dealing with thin barriers, or at a receiver point deep in the barrier's shadow zone. A recent paper by Habault and Filippi [11], who considered the effect of vibrating panels in rooms also suggests that this effect might influence noise barriers.

In a previous paper [6], the author presented a variational formalism for the study of two-dimensional (2-D) noise barriers, assumed to be either rigid or described by locally reacting impedances. In this paper, a fully coupled approach is presented. It is an extension of a formalism, based on a variational method using boundary elements, which was first developed by Jean in 1983 [12–14] and used by several authors in subsequent works [15–18]. An important review of numerical models to solve structural-acoustical problems can be found in reference [19].

The case of a simple barrier is considered. Three materials are tested: wood, glass or paraglass. The efficiency of the vibrating barrier is compared with that of a rigid barrier of the same thickness. At low frequencies, the vibration of very thin barriers affects their efficiency.

0022-460X/00/410001 + 21 $35.00/0

2. THE INTEGRAL REPRESENTATION

Figure 1 shows the geometry of the problem, A 2-D representation has been adopted, but the formalism is also valid in 3-D, provided that appropriate Green's functions are employed [13]. The analysis is done for harmonic time dependence $e^{-i\omega t}$. E is an infinite, coherent line source which, therefore, appears as a point source in the 2-D representation. The ground is flat, of infinite extent, and may be either rigid or of constant admittance α.

The integral representation of the pressure at any point M apart from the boundaries can be written as

$$P(M) = \int_S \left[\frac{\partial P(Q)}{\partial n_Q} G(M, Q) - P(Q) \frac{\partial G(M, Q)}{\partial n_Q} \right] dS(Q) + t(M). \tag{1}$$

$G(M, Q)$ is the Green solution of the problem; it gives the elementary pressure at any point M when only the infinite flat ground B is present, and for a unit line source at any point Q. $t(M)$ is the source contribution; it represents the pressure when only B is present. ρ is the fluid density. The integration is carried over the boundary S different from B; therefore S can either be a surface U above the ground such as a barrier or a part L of the ground having a different impedance than the ground B (for instance a portion of a road on an infinite grassy plane [7]).

n is the normal to the boundaries, directed towards the fluid. The admittances are defined as ratios of displacement to pressure.

The expression for G is the sum of three terms [3]:

$$G(M, Q) = -(i/4)H_0(kr) - (i/4)H_0(kr^-) + P_\alpha(M, Q). \tag{2}$$

Here r is the (M, Q) distance, r^- is the distance between M and the image of Q with respect to the ground B, and H_0 is the Hankel function of the first kind and order zero. The second

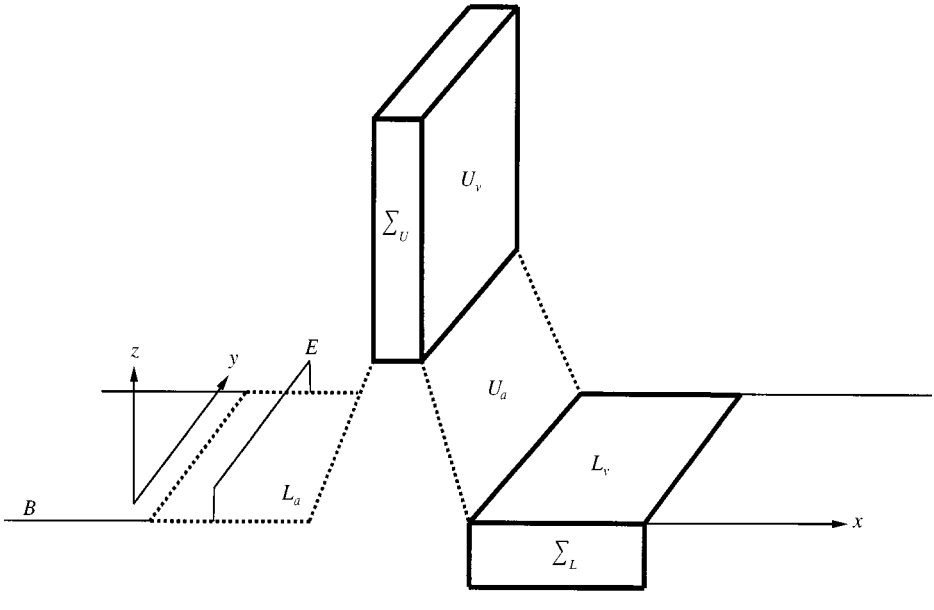

Figure 1. Geometry of the 2-D problem. L and U are lower and upper boundaries to be discretized. E is a coherent line source: Σ represents vibrating bodies; ▬, vibrating surface; - - - -, acoustical surface.

term describes the contribution of a hard floor, and P_α is the correction factor for ground admittance.

By definition, the elementary solution G verifies, on the plane $z = 0$, the relationship

$$\frac{\partial G(M, Q)}{\partial n_M} = \rho\omega^2 \alpha G(M, Q), \quad M \in B. \tag{3}$$

The surface of integration S (either above or on the ground) can be either defined as a vibrating surface or an acoustic surface (defined by its surface admittance), respectively, identified by the index v or a.

On $S_v = U_v \cup L_v$, the vibrating boundaries, one has

$$\partial P(Q)/\partial n_Q = \rho\omega^2 W(Q), \tag{4}$$

where W is the normal component of the displacement on the surface of the vibrating structure Σ.

On $S_a = U_a \cup L_a$, the boundaries of admittance Y, one has

$$\partial P(Q)/\partial n_Q = \rho\omega^2 Y(Q). \tag{5}$$

Substituting expressions (3)–(5) into equation (1) leads to a new expression for the pressure at any point M in the fluid:

$$\begin{aligned}\gamma(M)P(M) = &\int_{U_v}\left[\rho\omega^2 W(Q)G(M, Q) - P(Q)\frac{\partial G(M, Q)}{\partial n_Q}\right]\mathrm{d}S(Q)\\ &+ \int_{U_a} P(Q)\left[\rho\omega^2 Y(Q)G(M, Q) - \frac{\partial G(M, Q)}{\partial n_Q}\right]\mathrm{d}S(Q)\\ &+ \rho\omega^2 \int_{L_v} [W(Q) - \alpha P(Q)]\, G(M, Q)\,\mathrm{d}S(Q)\\ &+ \rho\omega^2 \int_{L_a} P(Q)[Y(Q) - \alpha]\, G(M, Q)\,\mathrm{d}S(Q) + t(M).\end{aligned} \tag{6}$$

$\gamma(M)$ is equal to unity for all points outside the upper boundary U and to $\frac{1}{2}$ for any smooth point on U.

In this expression, any integral containing a $\partial G/\partial n_Q$ term must be taken in the principal-value sense (PV).

One can then express $(1/\rho\omega^2)(\partial P/\partial n_M)$, when M is on S, as

$$D(M) + \begin{cases} -W(M)/2 \\ -Y(M)P(M)/2 \\ -\alpha P(M) \\ -\alpha P(M) \end{cases} = 0 \quad \text{if } M \in \begin{cases} U_v \\ U_a \\ L_v \\ L_a \end{cases}, \tag{7}$$

in which M is assumed to be a smooth point and

$$D(M) = FP \int_{U_v} \left[W(Q) \frac{\partial G(M,Q)}{\partial n_M} - P(Q) R(M,Q) \, \mathrm{d}S(Q) \right.$$
$$+ FP \int_{U_a} P(Q) \left[Y(Q) \frac{\partial G(M,Q)}{\partial n_M} - R(M,Q) \right] \mathrm{d}S(Q)$$
$$+ \int_{L_v} \left[W(Q) - \alpha P(Q) \frac{\partial G(M,Q)}{\partial n_M} \, \mathrm{d}S(Q) \right.$$
$$\left. + \int_{L_a} P(Q) [Y(Q) - \alpha] \frac{\partial G(M,Q)}{\partial n_M} \, \mathrm{d}S(Q) + \frac{1}{\rho \omega^2} \frac{\partial t(M)}{\partial n_M}, \right. \tag{8}$$

with

$$R(M,Q) = \partial^2 G(M,Q) / \partial n_M \partial n_Q. \tag{9}$$

The terms in expressions (7) are obtained, when M tends towards Q, as a limit contribution of $\partial G(M,Q)/\partial n_M$. FP denotes the finite part of the integral, which is divergent. The principal value PV is applied either to the L_v, L_u, U_a or U_v integral, depending on which of these surfaces M is on.

The functional for the fluid is then built in the case where there is no L_v, surface, since vibrating surfaces at ground level are unlikely to occur in the case of noise barriers. However, the computations can easily be done with this term included; this could correspond to the case of a vibrating plate in an infinite baffle.

In order to simplify the equations one can replace the integral operators by the notation $\langle \rangle_S$. Then one can introduce the arbitrary test function q, sufficiently regular and defined on the boundary S. The functional for the fluid is obtained by expressing

$$\langle q(M) Y(M) P(M) \rangle_{L_a}, \ \langle q(M) Y(M) P(M)/2 \rangle_{U_a}, \tag{10}$$

$$\langle q(M)(-\alpha P(M)) \rangle_{L_a}, \ \langle q(M)(-Y(M) P(M)/2) \rangle_{U_a}, \ \langle q(M) W(M)/2 \rangle_{U_v}. \tag{11}$$

In expression (10), $P(M)$ is obtained from equation (6) and, in expression (11), the expressions of equation (7) are employed. Each of these five quantities is then expressed as a homogeneous equation. Next, the functional of the fluid is obtained by summing these five homogeneous equations.

The functional $\mathbb{R}$ for the vibrating structure can be written as

$$\mathbb{R}(\mathbf{u}, \mathbf{W}) = E(\mathbf{u}, \mathbf{W}) - \langle P(u/2) \rangle_{U_v} - \langle u(P/2) \rangle_{U_v}. \tag{12}$$

E corresponds to the stiffness and mass terms of the structure whereas the simple integrals on the vibrating upper surface U_v correspond to the external loads due to the fluid. $\mathbf{W}$ represents the displacement vector and $\mathbf{u}$ is an associated test function (u is its normal component with respect to U_v). In the case of mechanical excitations, a $\langle \mathbf{u}.\boldsymbol{\varphi} \rangle_{U_v}$ term, in which $\boldsymbol{\varphi}$ represents the surface forces acting on U_v, must be added. In equation (12), the last term is modified by using expression (6) of P on U_v.

Finally, the total functional H is then the sum of equations (12), for the structure, and equations (10), (11) for the fluid,

$$H[(\mathbf{u}, q), (\mathbf{W}, P)] = E(\mathbf{u}, \mathbf{W}) + \Im[(u, q), (W, P)] = T(u, q),$$

in which $\Im$ is the fluid part of the functional expressed as

$$\Im[(u, q), (W, P)] = K(U_v, U_v) + K(U_a, U_a) + K(L_a, L_a) + K(U_a, U_v) + K(L_a, U_v) + K(U_a, \mathrm{L}_a) \tag{13}$$

and

$$T(u, q) = T(U_v) + T(U_a) + T(L_a).$$

The $K(A, B)$ terms are bilinear forms which correspond to the influence between boundaries A and B, the first three terms being auto-influence terms. The T terms are linear forms corresponding to the acoustical excitation. The expressions for the K and T terms are given in Appendix A. The terms $K(U_v, U_v)$ and $T(U_v)$ are often considered and correspond to the initial formulation by Jean [12, 13] but the addition of the other terms is necessary to obtain a general formulation to study noise barriers.

The bilinear form H is symmetric, since points M and Q may be interchanged. Therefore, $H[(\mathbf{W}, P), (\mathbf{u}, q)] = H[(\mathbf{u}, q), (\mathbf{W}, P)]$ and the solution $(\mathbf{W}, P)$ of the problem is the stationary point of

$$Z(\mathbf{W}, P) = \tfrac{1}{2} H[\mathbf{W}, P), (\mathbf{W}, P)] - T(\mathbf{W}, P). \tag{14}$$

In the previous expressions, the second integration takes care of the local values of $\gamma(M)$, at discontinous points, which are not equal to 1/2. The double integrations are all convergent, especially the integrals containing the double derivative R. The finite part of expressions (7), due to R, is suppressed by the second integration and the transformation [21] of the double derivative of G.

3. NUMERICAL IMPLEMENTATION

A finite-element technique was used to discretize equation (14). Two domains must be distinguished: the structure and the fluid.

The contribution of the fluid takes the form of surface integrals which, in 2-D, are contour integrals. Simple linear elements have been employed. Each double integral is written as a double sum over the Ne elements of the meshing. The fluid matrices are calculated by using a classical Gauss double summation. More detailed numerical considerations can be found in references [6, 13].

The contributions from the vibrating structure are calculated in the classical way, with full 2-D elements. Several elements have been implemented. In the case of the straight barrier considered in the examples, a six-node, 2-D-shell element is employed, with three nodes on each side [22]. It assumes that the normal stresses $\boldsymbol{\sigma}_n = 0$. In order to facilitate the implementation and construction of the global matrix, the stiffness and mass matrices corresponding to the structure are condensed, so that only the components corresponding to the nodes in contact with the fluid remain [13]. Upon calling Y the total matrix for the structure, and X the vector of mechanical excitations, if any, and denoting by c and u the coupled and uncoupled nodes, the reduced structural matrix and vector are

$$Y^* = Y_{cc} - Y_{cu} Y_{uu}^{-1} Y_{uc}, \qquad X^* = - Y_{cu} Y_{uu}^{-1} X_u. \tag{15}$$

Y^* can be obtained directly as an intermediate result of a triangular decomposition of Y, carried out only for the uncoupled nodes, where the coupled nodes are stored after the

uncoupled ones [23, 24]. The construction of the global matrix is then straightforward. When a material defined by its impedance is placed between a vibrating structure and the fluid, the corresponding normal displacement at the surface is stored as an unknown pressure. Due to the symmetry of the functional F, the global matrix is symmetrical.

The sizes of the elements for the boundaries, and for the structure itself, need not be the same, since the wavelengths at a given frequency can be different in the two domains, depending on the frequency with respect to the critical frequency. Rather than programming dedicated algorithms which permit the use of incompatible meshings, as in Reference [18], the case of a finer meshing for the structure has been addressed simply by using multiple meshings, and by suppressing the extra nodes on the coupled boundaries at the condensation state of the Y matrices. An example is given in the following paragraph. A Cholevsky decomposition of the matrix is used to solve the problem [25]. After resolution, equation (6) is used to obtain the pressure at any point in the fluid.

4. NUMERICAL EXAMPLES

The simple case of a straight barrier is considered. In most cases, the barrier is 3 m high and is made either of wood ($E = 12 \times 10^9$ N/m^2, $\rho_S = 650$ kg/m^3, $\eta = 0{\cdot}02$, $\nu = 0{\cdot}01$), of glass ($E = 87 \times 10^9$ N/m^2, $\rho_S = 2400$ kg/m^3, $\eta = 0{\cdot}001$, $\nu = 0{\cdot}24$)) or of paraglass ($E = 3{\cdot}3 \times 10^9$ N/m^2, $\rho_S = 1190$ kg/m^3, $\eta = 0{\cdot}03$, $\nu = 0{\cdot}40$), which is a type of plexiglass. The damping η is introduced in the form of a complex Young's modulus $E(1 + i\eta)$. These materials have been found to be representative of actual barrier designs. The barriers considered have small thickness values h, ranging from 10 to 30 mm. The x-axis is parallel to the ground and $x = 0$ is placed on the receiver side of the barrier such that the source side is at $x = -h$. The vertical co-ordinate z starts at the ground, which is first considered rigid. It should be noted that barriers made of paraglass tend to be more widely used in place of glass, usually with thickness $h = 10$ or 15 mm. A line source is placed at position $(-2{\cdot}3, 0{\cdot}5)$ and the sound pressure is computed at different positions behind the barrier at a height of 2 m. The fluid is air ($c = 340$ m/s, $\rho = 1{\cdot}3$ kg/m^3). These values are used in all cases unless otherwise stated.

4.1. MESHING

The elements used for the fluid and for the structure are presented in Figure 2. We call Nf and Ns the number of nodal interspaces on the vertical side, respectively, for the 2-node fluid elements and for the 6-node structural elements; in the case of Figure 2, $Nf = 6$ corresponds to three elements for the structure and $Ns = 6$.

Consider first the case of a 10-mm-thick glass barrier. At 200 Hz, the wavelength in air is 1·7 m and the bending wavelength in the barrier is only 0·682 m. Using 24 elements on each side of the barrier then corresponds to 13·6 elements per acoustical wavelength and 5·4 interspaces per bending wavelength. Figure 3 shows the pressure level at position (1, 2) obtained by using $Nf = 24$ or 48 elements for the fluid. In Figures 3(a) and 3(b) the numbers of structural elements are such that Ns is, respectively, equal to Nf and $Nf \times 4$ along the vertical side. As mentioned earlier, the use of a more refined meshing for the structure than for the fluid is rendered possible by condensing the extra nodes on the sides together with the interior nodes. Figure 3(a) shows that the peak at 215 Hz is not correctly estimated if $Ns = Nf = 24$. Figure 3(b) shows an improved convergence if Ns is increased by a factor of 4, since the results in those cases are little changed when the number of elements is multiplied by 2 ($Nf = 24$ or 48). This is particularly interesting, upon considering that the

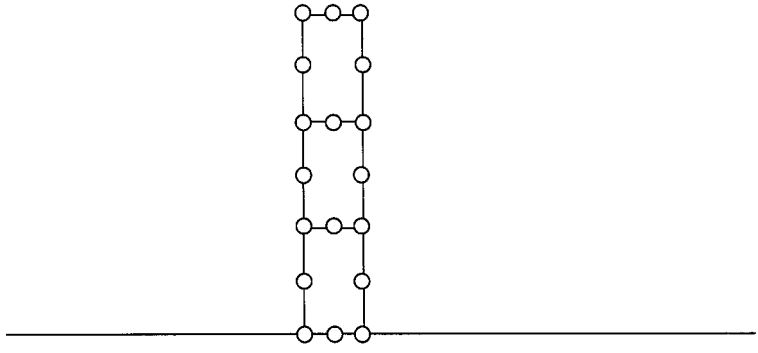

Figure 2. Meshing of a vertical barrier: three structural, six-node elements; six acoustical, 2-node elements on a vertical side.

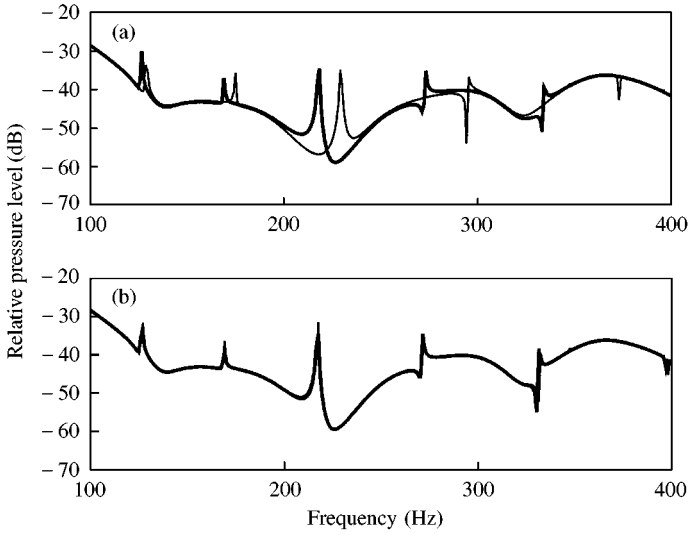

Figure 3. Effect of over-meshing the structure on the relative pressure level at point (1, 2). The fluid is meshed with nf —— 24 or —— 48 elements on a vertical side. The structure has (a), nf, (b) 4nf nodal corresponding interspaces. 10 mm glass barrier.

time needed to compute the fluid matrices is much higher than the time needed to compute the structural part of the problem. The 10-mm-thick paraglass barrier is the configuration most frequently used in the examples, and the computations are done with $Nf = 48, 96, 192$ and with $Ns = 2 \times Nf$. It has been verified that $Nf = 48$ ensures convergence up to 1500 Hz and that, with $Nf = 96$, convergence is obtained at 2000 Hz the highest third-octave band considered.

4.2. MODEL BEHAVIOUR

For the case of a 10-mm-thick barrier made of glass, the mean horizontal velocity level on the barrier, corresponding to bending, is plotted in Figure 4, along with the pressure level at position (1, 1), for both the vibrating and the rigid cases. The source is a unit coherent line. The peaks in the velocity spectrum correspond to the bending behaviour of the barrier; peak

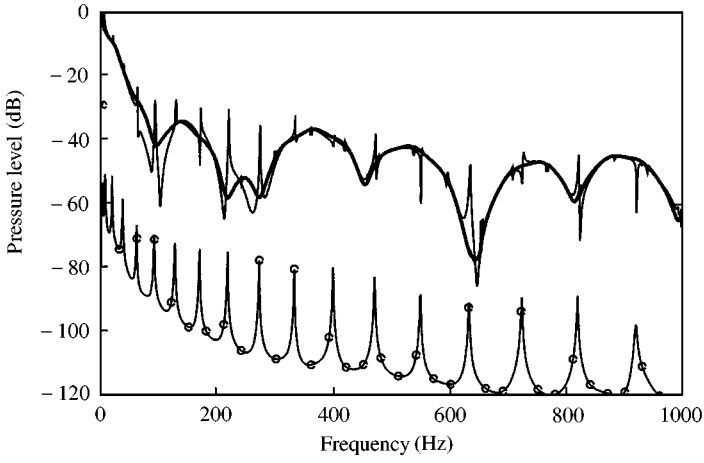

Figure 4. Modal behaviour of a 10 mm glass barrier: ○——○ mean bending velocity; pressure level at (1, 1); —— glass barrier ——— rigid barrier.

values can also be seen in the pressure response of the vibrating barrier. Apart from the peaks, the pressure level of the rigid barrier is close to that generated by the vibrating barrier at high frequencies whereas, between 50 and 300 Hz, larger differences can be noticed. The first bending modes occur at 6·5, 18, 36·5, 60·5, 90·5, 126·5, 169 and 217 Hz. Around 200 Hz (bending wavelength 1·061 m), where the maximal influence of the barrier's elasticity can be seen (see also Figure 6), there are already several bending wavelengths along the barrier so that no clear relationship can be established between structural wavelength and maximal effect of the barrier's elasticity. For other more damped materials, such as paraglass, the modal behaviour of the barrier cannot be seen so clearly on the pressure levels.

4.3. EFFECT OF THE BARRIER MATERIAL

The effect of the vibrations is best estimated as the difference between the pressure levels in the vibrating and rigid cases, which we shall call the relative pressure level. In Figure 5–7, such differences are plotted, at positions 5 and 20 m behind the screen, and at $z = 2$ m, for 10-mm-thick barriers, respectively, made of wood, glass and paraglass. Note that each figure has a different vertical scale. A positive value corresponds to an increase of pressure level behind the barrier or a reduction of the barrier's efficiency and is mainly due to the occurrence of structural resonances, whereas anti-resonances will have an opposite effect. The highest level differences are found for wood; the sharpest peaks are obtained for the glass material which is the least damped. However, in practice, wooden barriers are usually thicker than 10 mm, at least in the order of a few centimetres.

4.4. EFFECT OF THE BARRIER THICKNESS

Figures 8–10 show, in third-octave bands and at position (20, 2), the relative pressure levels, respectively, for the three materials, for thicknesses of 10, 20 and 30 mm. Above 20 mm, the effect is less than 3 dB at all frequencies. For all barriers, the strongest effect is seen at 200 and 250 Hz. This is significant, since the contribution of lorries to traffic noise is

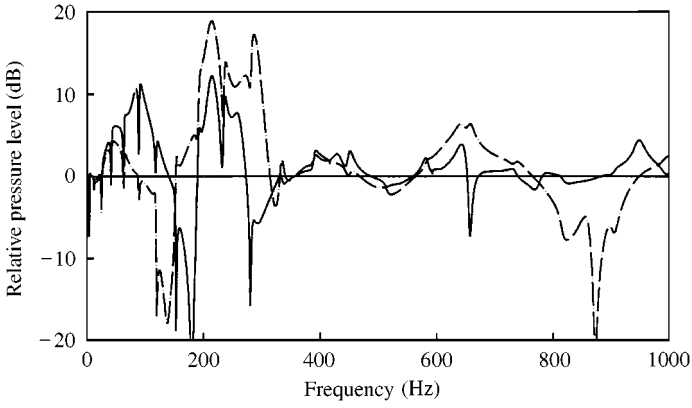

Figure 5. Effect of barrier material on its efficiency: —— 5 m and – · – · – · – 20 m behind the barrier, at $z = 2$ m. Barrier made of wood, 3 m high, 10 mm thick.

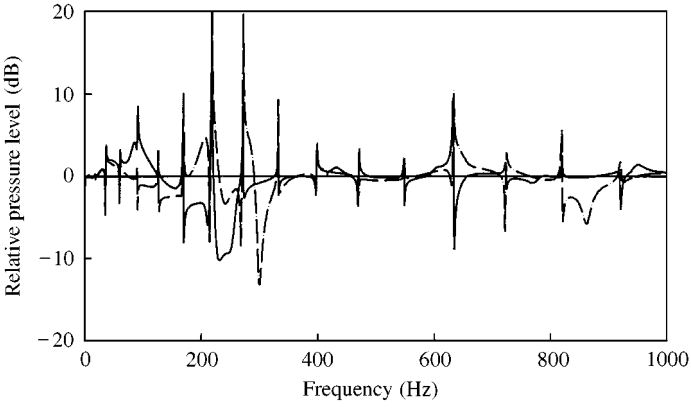

Figure 6. Effect of barrier material on its efficiency: —— 5 m and – · – · – · – 20 m behind the barrier, at $z = 2$ m. Barrier made of glass, 3 m high, 10 mm thick.

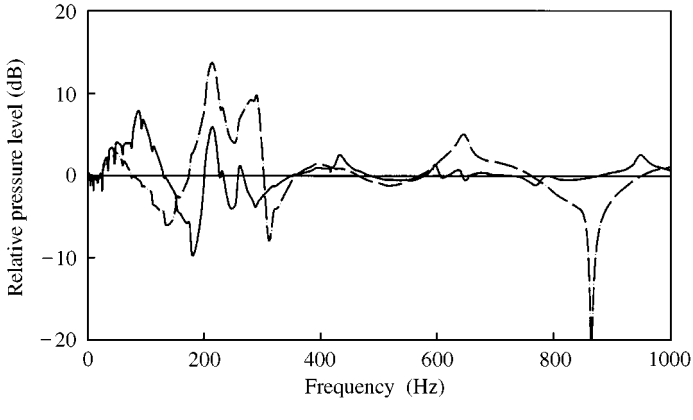

Figure 7. Effect of barrier material on its efficiency: —— 5 m and – · – · – · – 20 m behind the barrier, at $z = 2$ m. Barrier made of paraglass, 3 m high, 10 mm thick.

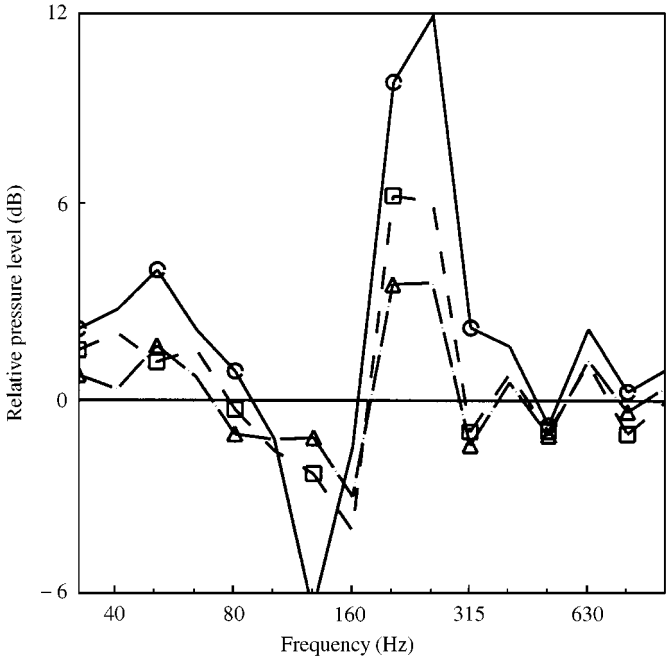

Figure 8. Effect of the thickness of the barrier on the relative pressure level. Third-octave band results. Receiver at (20, 2). Wooden barrier: ○——○ 10 mm; □– – –□ 20 mm; △–·–·–△ 30 mm.

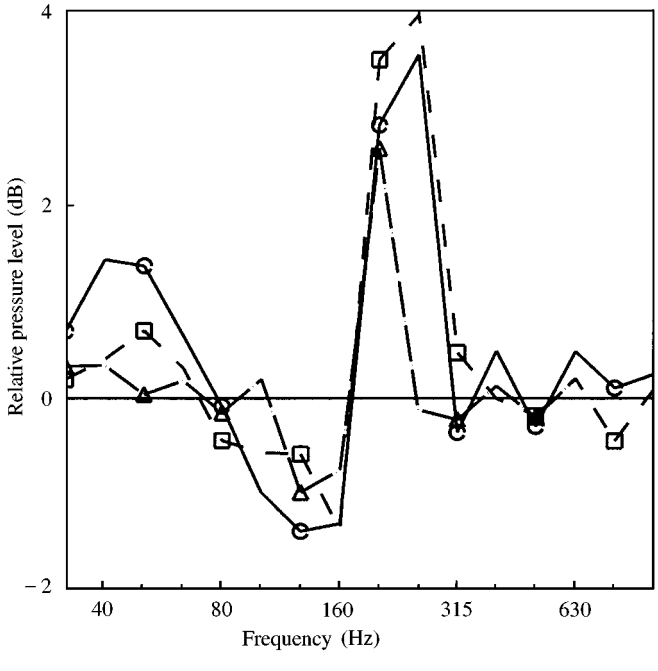

Figure 9. Effect of the thickness of the barrier on the relative pressure level. Receiver at (20, 2). Glass barrier: ○——○ 10 m; □– – –□ 20 mm; △–·–·–△ 30 mm.

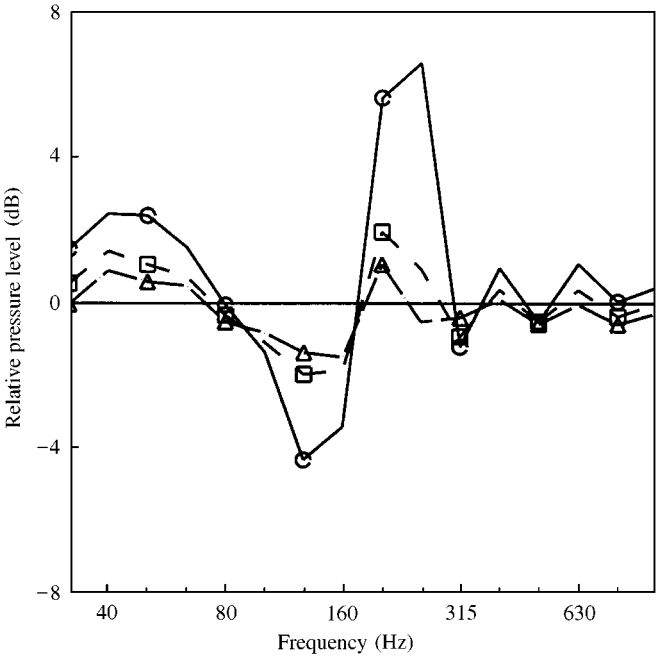

Figure 10. Effect of the thickness of the barrier on the relative pressure level. Receiver at (20, 2). Paraglass barrier: ○——○ 10 mm; □– – –□ 20 mm; △–·–·–△ 30 mm

becoming more and more important; the vibration of such barriers can be significantly affected by the low-frequency acoustical emission of these vehicles. The noise emitted by motorbikes is also important around 200–250 Hz.

4.5. EFFECT OF THE INTERNAL LOSS FACTOR

The three materials considered in Figures 5–10 have different loss factors, and the effect of various values of η is now considered, for glass and paraglass barriers, by taking $\eta = 0{\cdot}001$ (as for glass in Figures 6 and 9), and 0·03 (as for paraglass in Figures 7 and 10). As can be seen in Figures 11(a) and 11(b), respectively, for glass and for paraglass, increasing η will smooth the relative pressure levels without changing the general trends of the curves. Corresponding third-octave results, as shown in Figures 12(a) and 12(b), reveal little influence of η in the case of paraglass whereas, in the case of glass barriers, the main effect at 200 Hz, already less important than for paraglass, becomes even less pronounced if η changes from 0·001 to 0·01. In practice, when glass panels are mounted in supporting structures, extra damping is added by the boundary conditions, resulting in higher values. Measurements have been carried out [26] on actuglass 4-m-high barriers. Reverberation time measurements using impact excitation have led to values of η in the order of 0·03 below 500 Hz. Measurements on 2 mm steel barriers have led to values of η in the order of 0·04.

4.6. EFFECT OF RECEIVER AND SOURCE POSITION

The effect of the elasticity of the barrier depends on the receiver position. For the 10-mm-thick paraglass barrier, the third-octave relative pressure levels are plotted in Figures 13(a)–13(c). Each plot corresponds to a different third-octave band and shows

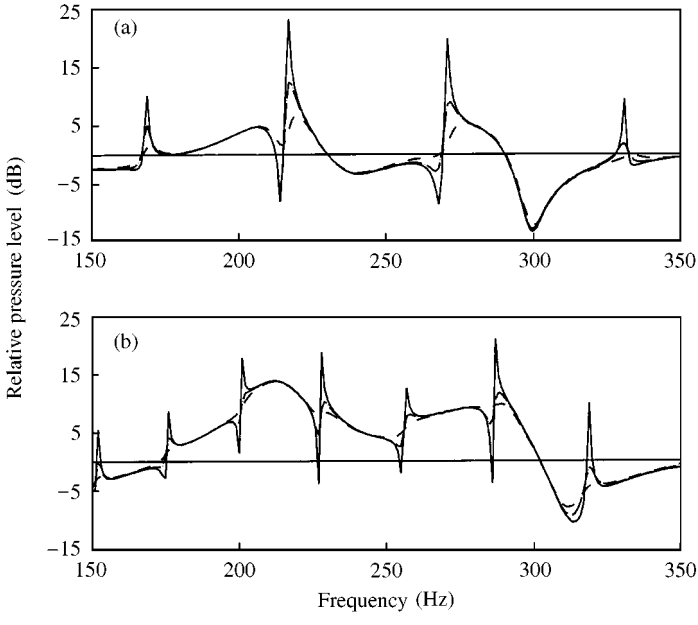

Figure 11. Effect of different values of η: (a) glass barrier; (b) paraglass barrier; —— $\eta = 0{\cdot}001$; – · – · – $\eta = 0{\cdot}01$; - - - - - $\eta = 0{\cdot}03$.

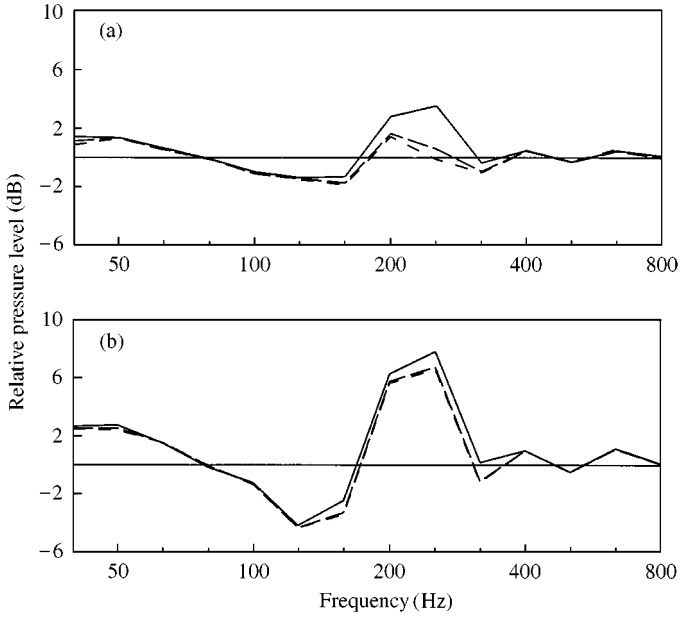

Figure 12. Effect of different values of η: (a) glass barrier; (b) paraglass barrier; —— $\eta = 0{\cdot}001$; – · – · – $\eta = 0{\cdot}01$; - - - - - $\eta = 0{\cdot}03$. Third-octave results.

the pressure-level differences at 2 m height and at distances varying from 1 to 50 m behind the barrier. The highest values are found at 200 Hz and reach a maximum 14 m behind the barrier. At other frequencies the maximum effect occurs at other positions. For instance, at 630 Hz, a maximal effect is found 44 m behind the barrier.

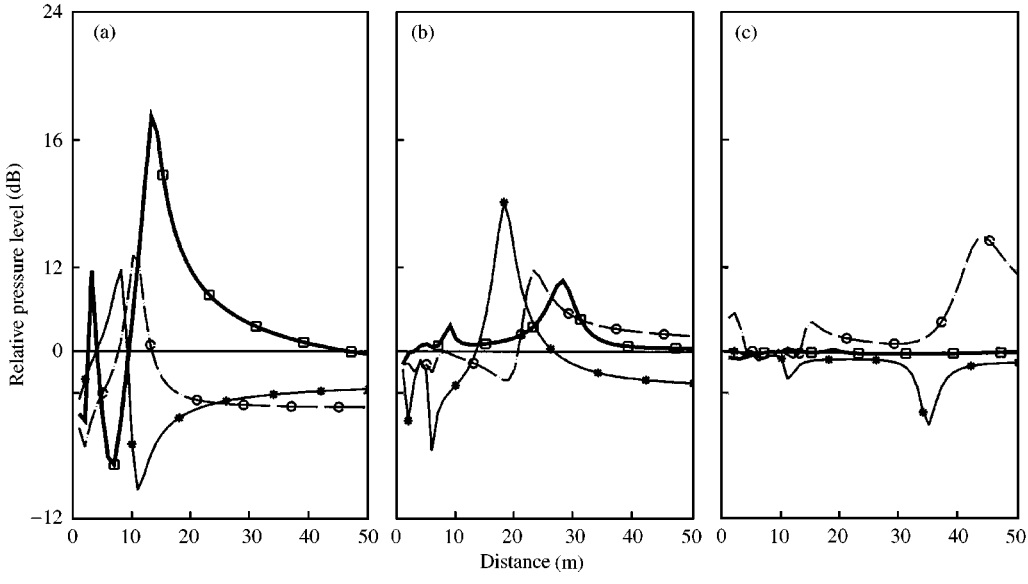

Figure 13. Relative pressure level as a function of the distance behind the barrier, at $z = 2$ m. Paraglass 10 mm: *——*, ○–·–·–○, ——, (a) 125, 160, 200 Hz; (b) 250, 315, 400 Hz; (c) 500, 630, 800 Hz.

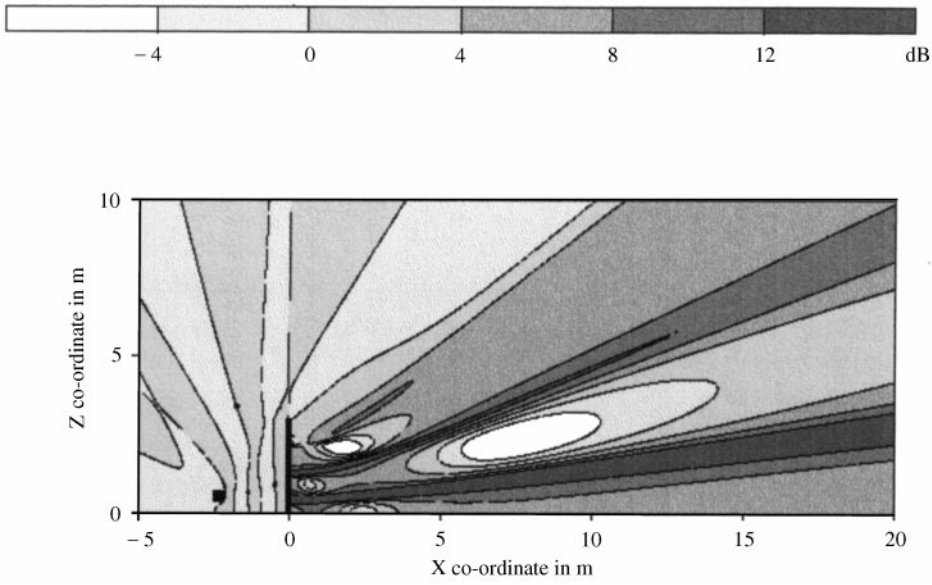

Figure 14. Relative pressure level, third-octave 200 Hz. Paraglass 10 mm, receiver at $z = 2$ m.

The variation of the vibration effects with receiver position is best appreciated by looking at Figure 14 which shows, in the 200 Hz third-octave band, the variation of the relative pressure level as a function of both the x and z positions behind the barrier. A strong angular dependence can be seen, since maximum effects appear along regular lines starting at the barrier. Along the most important of these lines the amplitude exceeds 12 dB.

The effect of the position of the source is illustrated in Figures 15(a) and 15(b), for the case of a 10-mm-thick paraglass barrier, and for a receiver, respectively, at (5, 2) or (20, 2). The

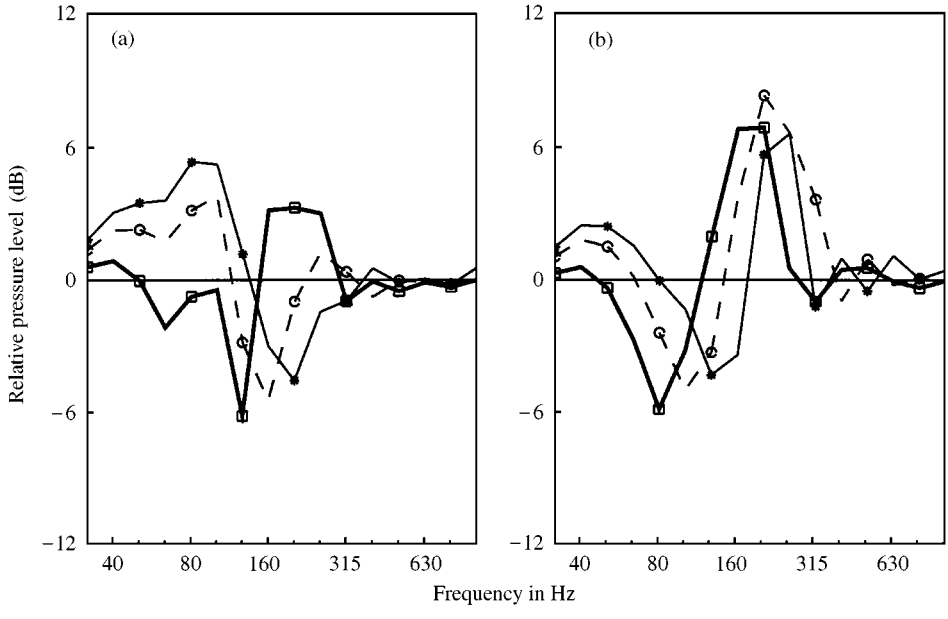

Figure 15. Effect of the position of the source. Paraglass 10 mm, receiver at (a) (5, 2), (b) (20, 2) S at $x =$ ∗——∗ −2·29, ○— —○ −1·29, ▬▬ −0·49.

source is placed successively at $x = -2{\cdot}29$, $-1{\cdot}29$ and $-0{\cdot}49$ m, at $z = 2$ m. The effect of position is very marked; no systematic variation can be seen.

4.7. EFFECT OF THE BARRIER HEIGHT

Next, the effect of the height of the barrier is investigated. This height is taken as 2, 3 and 4 m, for a paraglass barrier, 10 mm thick. The sound pressure level at point (20, 2) is plotted successively in Figures 16(a), 16(b) and 16(c) for the three heights, both for a rigid barrier and a vibrating barrier. As already noted, vibrations of the barrier will affect the sound pressure in the low-frequency range. In the case of the 4-m-high barrier (Figure 16(c)), the minimum value of the pressure level at 200 Hz is well compensated by the action of the vibrations such that the importance of a source with a strong emission component at this frequency, might be underestimated if the barrier is assumed to be rigid.

The variation of the relative pressure level with the distance behind the 4-m-high barrier, in the third-octave bands 125, 160 and 200 Hz, is plotted in Figure 17, and should be compared to Figure 13(a) obtained for a 3-m-high barrier. The increase of the effect of the barrier's elasticity is apparent at most positions; it becomes principally a positive effect whereas, for the 3-m-high barrier, negative values can be seen at many frequencies.

Figure 18 shows, again, the effect of position of the receiver behind the barrier by comparing the absolute pressure levels for the rigid and the paraglass barriers, for third-octave levels 125 to 250 Hz and confirms the positive effects noticed in Figure 17.

4.8. OTHER EFFECTS

In the previous examples the ground has been taken as rigid. The effect of a ground covered with grass ($\sigma = 600$ kN s/m^4 in the Delany and Bazley model [27]) is illustrated in

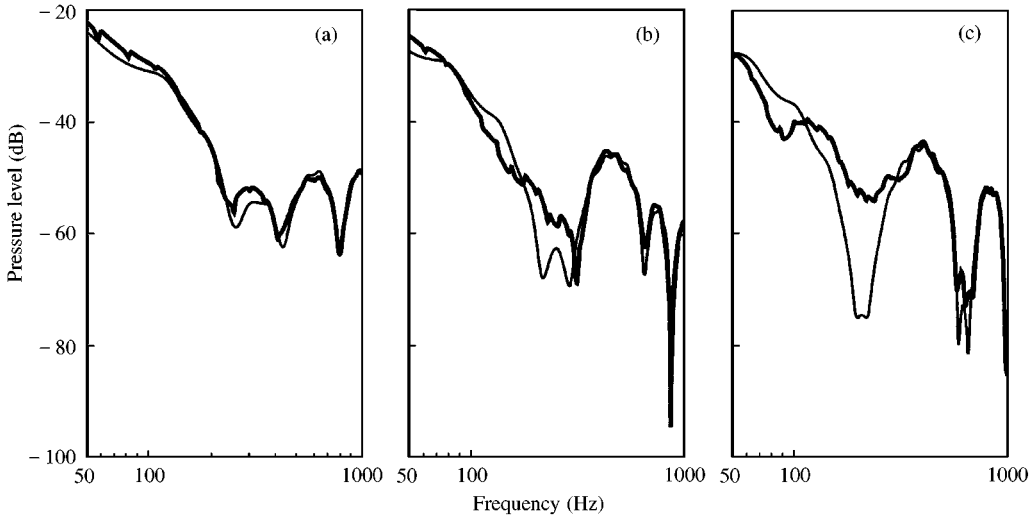

Figure 16. Effect of the barrier height, at (20, 2): —— rigid; —— 10 mm paraglass. Heights (a) 2 m, (b) 3 m, (c) 4 m.

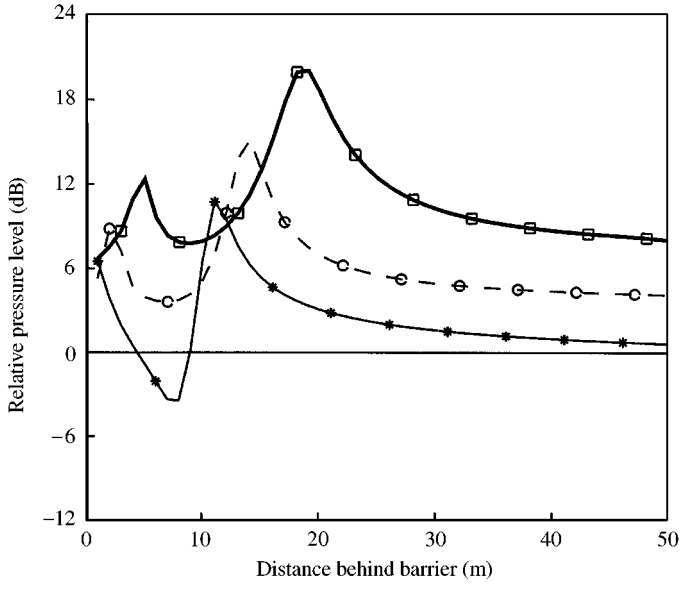

Figure 17. Relative pressure level as a function of the distance behind the barrier, at $z = 2$ m. Paraglass 10 mm, 4 m high: ∗——∗; ○——○; □——□ 125, 160, 200 Hz.

Figure 19. The relative pressure level at 200 Hz, behind the barrier, is plotted for both the rigid and grass situations. Little difference can be seen, so that the type of ground does not seem to affect the previous results.

The influence of an absorbent material placed on the barrier is now considered. A 3 m high and 10 mm thick barrier, either rigid or made of paraglass, is prolonged by 1 m of an impedant structure ($\sigma = 30$ kN s/m^4) of the same thickness. In the case of the elastic lower part with an absorbent upper part, surfaces S_v and S_a must be considered in the functional

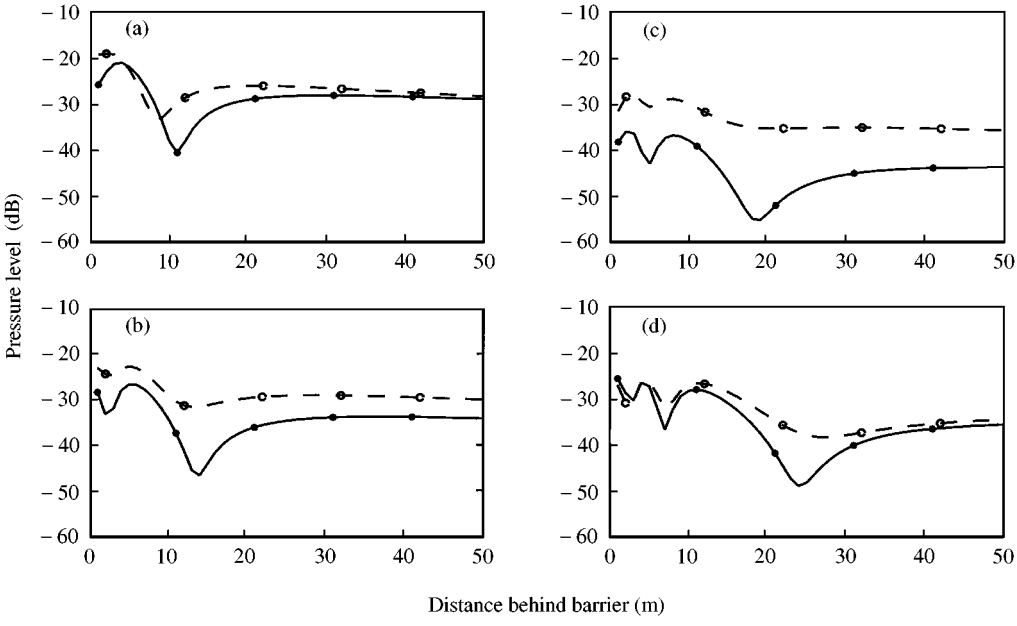

Figure 18. Pressure level as a function of the distance behind the barrier, at $z = 2$ m. Barrier 10 mm thick and 4 m high: ∗——∗ rigid; ○——○ paraglass. (a), (b), (c), (d) 125, 160, 200, 250 Hz.

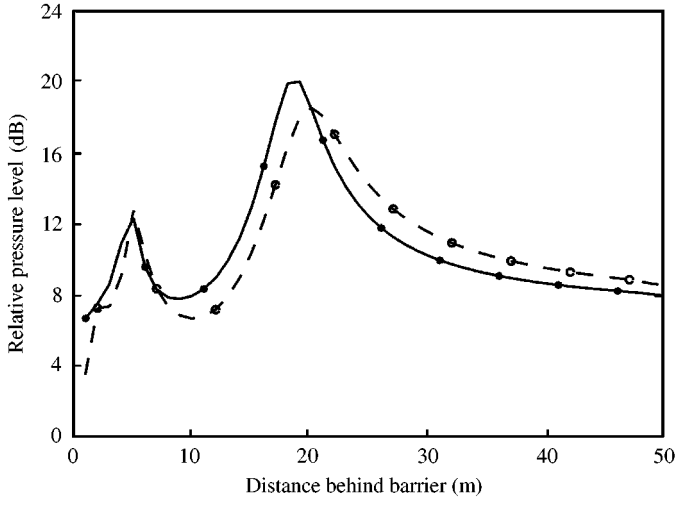

Figure 19. Effect of the ground impedance on the relative pressure level behind the barrier, at $z = 2$ m. 200 Hz. 4 m high barrier, paraglass 10 mm: ∗——∗ rigid ground; ○——○ grass ($\sigma = 600$ kN s m^{-4}).

(terms (A.1)–(A.5) in Appendix A). Figure 20 reports, for both the rigid (Figure 20(a)) and paraglass (Figure 20(b)) lower parts, a comparison of the pressure levels obtained for the 3 m and 3 + 1 m high barriers, at point (20, 2). Different efficiencies of the extra 1 m absorbent extension are obtained for the rigid and elastic situations. In the rigid case, the addition of 1 m of absorbent length results in a shift of interference patterns towards the low frequencies, so that the pressure levels are increased between 250 and 400 Hz, whereas for

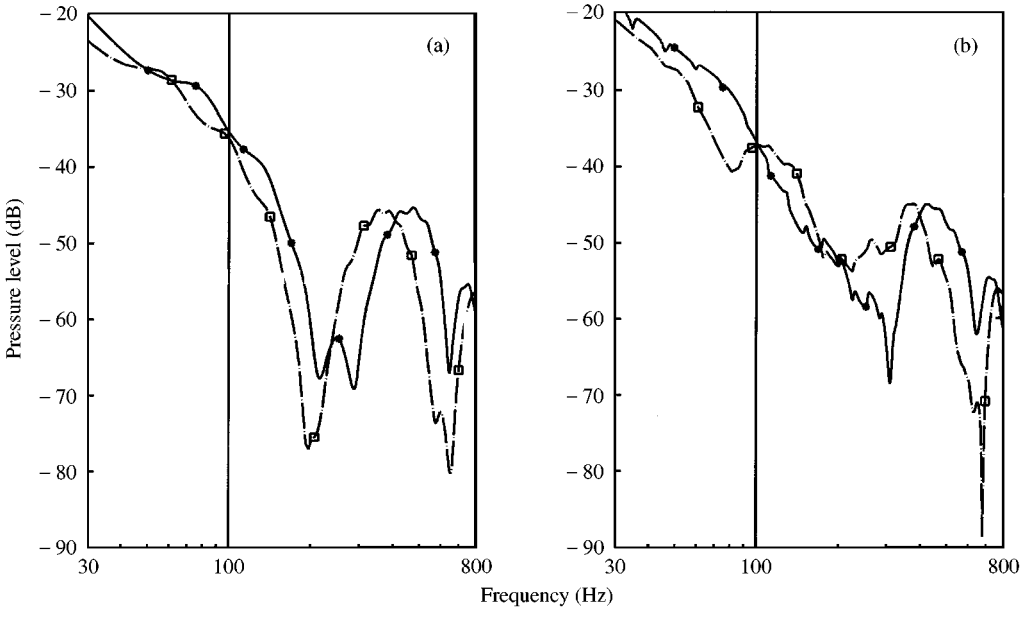

Figure 20. Effect of a 1 m absorbent extension ($\sigma = 30$ kN s m^4) of a 3 m high 10 mm thick barrier. (a) rigid (b) paraglass. Receiver at (20, 2): ∗——∗ 3 m, □–·–·–·–□ 3 m + 1 m.

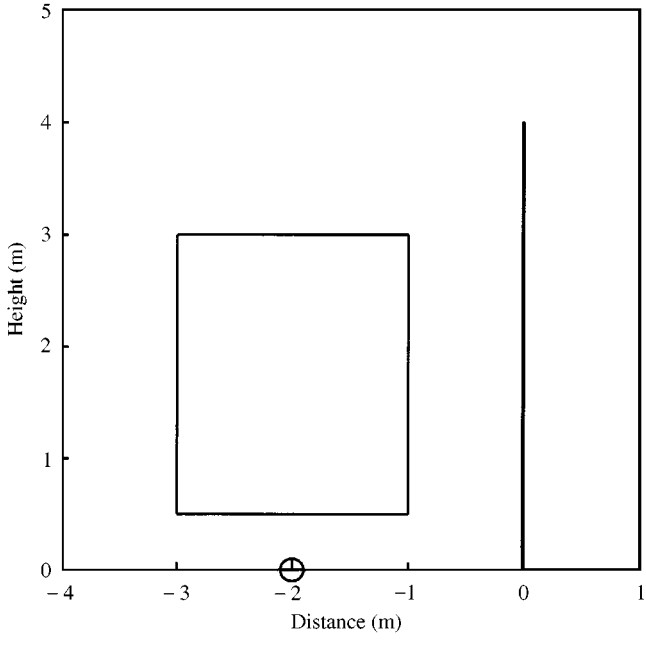

Figure 21. Case of a source at $(-2, 0)$ under a rigid lorry. 10 mm thick barrier.

the elastic case, the pressure level is increased between 100 and 400 Hz when the barrier length is increased.

The last situation considered is related to the presence of a lorry close to the noise barrier (Figure 21). A source is placed under the lorry, at ground level at position $(-2, 0)$.

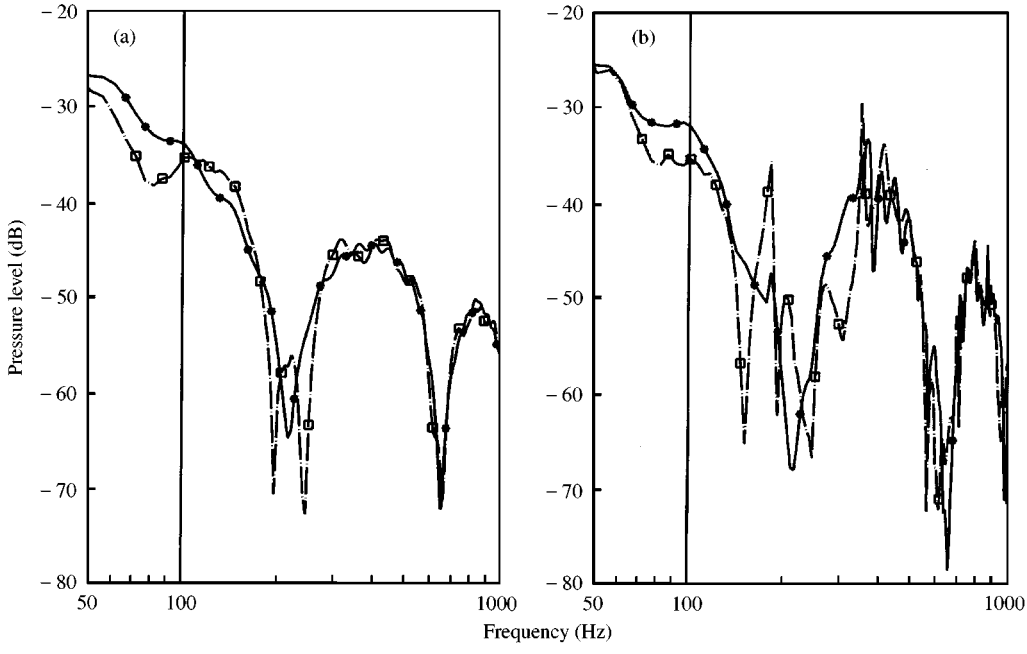

Figure 22. Effect of a lorry. Receiver at (20, 2), 10 mm barrier: (a) no lorry; (b) with the lorry: ∗——∗ rigid; – · – · – · – paraglass.

Computations have been made both without and with the lorry, in the case of a 4 m high, 10 mm thick barrier, either rigid or made of paraglass. The pressure levels have been estimated at position (20, 2). Figure 22 compares the rigid and elastic barriers both without (Figure 22(a)) and with the lorry (Figure 22(b)). It is interesting to note that when the lorry is added, the effect of the barrier's elasticity is more pronounced. Due to the multiple reflections between the barrier and the lorry and also due to a change of the angle of incidence of the waves impinging on the top of the barrier, the relative effect of the vibrations of the barrier is then more important.

5. CONCLUSION

The importance of traffic noise emphasizes the role of noise barriers. New designs appear constantly as attempts to optimize the cost/efficiency/design compromise. Thin barriers—of the order of only 10 or 15 mm thick—made of paraglass are more and more frequently employed. Traditional numerical predictions neglect the vibration behaviour of noise barriers, assuming that the transmission is predominantly determined by diffraction effects. This assumption has been checked by using a variational approach combined with boundary elements for the fluid, and classical finite elements for the vibrating structure. Low-frequency effects have been revealed, typically around 200 Hz and in excess of 5 dB in this frequency band in the case of thin paraglass barriers. The effect of the vibrations usually occurs at the frequencies at which the rigid barrier shows minimum pressure levels; thus a levelling of the frequency response results from the consideration of the vibro-acoustical behaviour. Using a global dB(A) indicator would not show significant differences between rigid and vibrating noise barriers. The relevance of such an indicator is worth considering,

especially with the prospect of increasing low-frequency noise from lorries. The program developed for this study is general in nature and can easily account for complex situations. Using a 2-D approach permits easy and fast parametric studies, with little effort necessary for the input and post-processing of data. Other factors, such as porous media or atmospheric conditions, should be considered in future work.

REFERENCES

1. T. Okubo and K. Fujiwara 1998 *Journal of Sound and Vibration* **216**, 771–790. Efficiency of a noise barrier on the ground with an acoustically soft cylindrical edge.
2. D. C. Hothersall, S. N. Chandler-Wilde and M. N. Hajmirzae 1991 *Journal of Sound and Vibration* **146**, 303–322. Efficiency of single noise barriers.
3. S. N. Chandler-Wilde and D. C. Hothersall 1995 *Journal of Sound and Vibration* **180**, 705–724. Efficient calculation of the Green function for acoustic propagation above a homogeneous impedance plane.
4. D. Duhamel 1996 *Journal of Sound and Vibration* **197**, 547–571. Efficient calculation of the three-dimensional sound pressure field around a noise barrier.
5. D. Duhamel and P. Sergent 1998 *Journal of Sound and Vibration* **218**, 799–823. Sound propagation over noise barriers with absorbing ground.
6. P. Jean 1998 *Journal of Sound and Vibration* **212**, 275–294. A variational approach for the study of outdoor sound propagation and application to railway noise.
7. P. Jean, G. Defrance and Y. Gabillet 1999 *Journal of Sound and Vibration* **226**, 201–216. The importance of source type on the assessment of noise barriers.
8. P. A. Morgan, D. C. Hothersall and S. N. Chandler-Wilde 1998 *Journal of Sound and Vibrations* **217**, 405–417. Influence of shape and absorbing surface—a numerical study of railway noise barriers.
9. E. Premat and Y. Gabillet *Journal of the Acoustical Society of America*. Using a boundary element method for predicting noise barriers efficiency with meteorological effects. (Accepted for publication).
10. Y. Gabillet, H. Schroeder, G. A. Daigle and A. L'Esperance 1993 *Journal of Acoustical Society of America* **93**, 3105–3116. Application of the Gaussian beam approach to sound propagation in the atmosphere: theory and experiments.
11. D. Habault and P. J. T. Filippi 1998 *Journal of Sound and Vibration* **213**, 333–374. Light fluid approximation for sound radiation and diffraction by thin elastic plates.
12. P. Jean June 1983 *Intermediate Doctorate Report*, *Université de Technologie de Compiègne*. Une formulation variationnelle pour l'étude du couplage vibro-acoustique en présence d'un écoulement uniforme constant. [A variational formulation for the study of elasto-acoustical coupled problems in the presence of a constant uniform flow].
13. P. Jean 1985 *Thèse de doctorat*, *Université de Technologie de Compiègne*. Une méthode variationnelle par équations intégrales pour la résolution numérique de problèmes intérieurs et extérieurs de couplage élasto-acoustique. [A variational formalism using integral equations for the numerical resolution of interior and exterior elasto-acoustical coupled problems. (English translation available upon request).]
14. M. A. Hamdi and P. Jean 1985 *Colloque Tendances actuelles en calcul des structures Bastia*, 6–8 *Novembre*. Résolution numérique des problèmes couplés par une méthode d'eléments finis de frontière.
15. C. Lesueur 1988 *Rayonnement Acoustique des Structures*. Collection de la DER, EDF, Eyrolles.
16. R. A. Jeans and I. C. Mathews 1990 *Journal of the Acoustical Society of America* **88**, 2459–2466. Solution of fluid–structure interaction problems using a coupled finite element and variational element technique.
17. H. Defosse, M. A. Hamadi and L. Mebarek *Proceedings of International Conference on Aeroacoustics and Dynamic Environment of Space Transportation Systems*, *Jouy-en-Josas*, *France*, 8–11 *February* 1994. Coupling of integral and finite element methods for solving vibroacoustic problems.
18. M. Guerich and M. A. Hamdi 1999 *Journal of Acoustical Society of America* **105**, 1682–1694. A numerical method for vibro-acoustic problems with incompatible finite element meshes using B-spline functions.

19. N. ATALLA and R. J. BERNHARD 1994 *Applied Acoustics* **43**, 271–294. Review of numerical solutions for low-frequency structural acoustic problems.
20. R. D. CISKOWSKI and C. A. BREBBIA 1991 *Boundary Element Methods in Acoustics*. Computational Mechanics Publications Elsevier Applied Science.
21. C. MONKALA 1988 *Thèse de doctorat*, *Université de Technologie de Compiègne*. Effet des singularités géometriques sur les résultats numériques d'une méthode d'éléments finis de frontière dans un problème plan.
22. P. HUBERT 1986 *Finite element program CESAR. Manuel thérique. Laoratoire Central des Ponts et Chaussées*.
23. P. DANGLA 1988 *Earthquake and Structural Dynamics* **16**, 115–1128. A plane-strain soil–structure interaction model.
24. P. JEAN *Acta Acustica*. Boundary elements for 2D soil–structure interaction problems (accepted for publication).
25. W. H. PRESS, S. A. TEUKOLSKY, W. T. WETTERING and B. P. FLANNERY 1994 *Numerical Recipes*. Cambridge: Cambridge University Press.
26. J. DEFRANCE and Y. GABILLET 1997 E.C. *Measurements and testing programme*, *Project MAT1-CT94049 "ADRIENNE". Partner* 3.2 *CSTB. Doc.ADR*3-2-.5. Structural reverberation time measurements.
27. M. E. DELANY and E. N. BAZLEY 1970 *Applied Acoustics* **3**, 105–116. Acoustical properties of fibrous absorbent materials.

APPENDIX A: FLUID FUNCTIONAL

The fluid terms of the functional are denoted by $K(A, B)$ and $T(A)$, where A and B denote either U_v (the total vibrating surface above the ground), U_a (the impedant surface above the ground) or L_a (any portion of the ground characterized by impedant conditions other than that of the infinite flat ground). The K terms, after discretization will contribute to the total matrix whereas the T terms will contribute to the solicitation vector. W and P denote, respectively, the normal displacement of a vibrating surface and the acoustic pressure. u and q are associated test functions.

The first two terms correspond to the case of a vibrating structure above the ground and will be the only terms to be retained if there are no impedant surfaces:

$$\begin{aligned} K(U_v, U_v) = &- \langle\langle \rho\omega^2 u(M) G(M, Q) W(Q)\rangle\rangle_{U_v \times U_v} + \langle\langle u(M)(\partial G(M, Q)/\partial n_Q)) P(Q)\rangle\rangle_{U_v \times U_v} \\ &\langle\langle q(M)(\partial G(M, Q)/\partial n_M) W(Q)\rangle\rangle_{U_v \times U_v} - \langle\langle q(M) R(M, Q) P(Q)\rangle\rangle_{U_v \times U_v} \\ &- \langle u(M)(P(M)/2)\rangle_{U_v} - \langle q(M)(W(M)/2)\rangle_{U_v}, \end{aligned} \tag{A.1}$$

$$T(U_v) = \langle u(M) t(M)\rangle_{U_v} - \langle q(M)\bar{t}(M)\rangle_{U_v}, \tag{A.2}$$

in which $\bar{t} = (1/\rho\omega^2)(\partial t/\partial n_M)$.

Terms (A.3)–(A.5) must be considered whenever there is an absorbent surface above the ground:

$$\begin{aligned} K(U_a, U_a) = &- \langle\langle \rho\omega^2 q(M) Y(M) G(M, Q) Y(Q) P(Q)\rangle\rangle_{U_a \times U_a} \\ &+ \langle\langle q(M)[Y(M)(\partial G(M, Q)/\partial nQ) + (Y(Q)(\partial G(M, Q)/\partial n_M)] P(Q)\rangle\rangle_{U_a \times U_a} \\ &- \langle\langle q(M) R(M, Q) P(Q)\rangle\rangle_{U_a \times U_a}, \end{aligned} \tag{A.3}$$

$$\begin{aligned} K(U_a, U_v) = &+ \langle\langle u(M)[(\partial G(M, Q)/\partial n_Q) - \rho\omega^2 Y(Q) G(M, Q)] P(Q)\rangle\rangle_{U_a \times U_v} \\ &+ \langle\langle q(M)[(\partial G(M, Q)/\partial n_M) - \rho\omega^2 Y(M) G(M, Q)] W(Q)\rangle\rangle_{U_v \times U_a} \end{aligned}$$

$$+ \langle\langle q(M)[Y(Q)\partial G(M,Q)/\partial n_M - R(M,Q)]P(Q)\rangle\rangle_{U_a\times U_v}$$

$$+ \langle\langle q(M)[Y(M)\partial G(M,Q)/\partial n_Q - R(M,Q)]P(Q)\rangle\rangle_{U_v\times U_a}, \tag{A.4}$$

$$T(U_a) = \langle q(M)\,Y(M)t(M)\rangle_{U_a} - \langle q(M)\bar{t}(M)\rangle_{U_a}. \tag{A.5}$$

The remaining expressions must be considered if part of the ground differs from the infinite ground and must therefore be discretized [7]:

$$K(L_a, L_a) = -\langle\langle q(M)(Y(M)-\alpha)(Y(Q)-\alpha)P(Q)\rangle\rangle_{L_a\times L_a} + \langle q(M)(Y(M)-\alpha)P(M)\rangle_{L_a},$$

$$T(L_a) = \langle q(M)\,Y(M)t(M)\rangle_{L_a} - \langle q(M))\bar{t}(M)\rangle_{L_a}, \tag{A.6}$$

$$K(L_a, U_v) = -\langle\langle u(M)\rho\omega^2(Y(Q)-\alpha)G(M,Q)P(Q)\rangle\rangle_{L_a\times U_v}$$

$$-\langle\langle q(M)\rho\omega^2(Y(M)-\alpha)G(M,Q)W(Q)\rangle\rangle_{U_v\times L_a}$$

$$+\langle\langle q(M)(Y(Q)-\alpha)(\partial G/\partial n_M)P(Q)\rangle\rangle_{L_a\times U_v}$$

$$+\langle\langle q(M)(Y(M)-\alpha)(\partial G/\partial nQ)P(Q)\rangle\rangle_{U_v\times L_a}, \tag{A.7}$$

$$K(L_a, U_a) = \langle\langle q(M)(Y(Q)) - \alpha)[(\partial G/\partial n_M) - \rho\omega^2 Y(M)G(M,Q)]P(Q)\rangle\rangle_{L_a\times U_a}$$

$$+\langle\langle q(M)(Y(M)-\alpha)[(\partial G/\partial n_Q) - \rho\omega^2 Y(Q)G(M,Q)]P(Q)\rangle\rangle\rangle\rangle_{U_a\times L_a}. \tag{A.8}$$